Nanostraws for Direct Fluidic Intracellular Access

Jules J. VanDersarl,[‡] Alexander M. Xu,[‡] and Nicholas A. Melosh*

Department of Materials Science and Engineering, Stanford University, Stanford, California 94305, United States

S Supporting Information

ABSTRACT: Nanomaterials are promising candidates to improve the delivery efficiency and control of active agents such as DNA or drugs directly into cells. Here we demonstrate cell-culture platforms of nanotemplated "nanostraws" that pierce the cell membrane, providing a permanent fluidic pipeline into the cell for direct cytosolic access. Conventional polymeric track-etch cell culture membranes are alumina coated and etched to produce fields of nanostraws with controllable diameter, thickness, and height. Small molecules and ions were successfully transported into the cytosol with 40 and 70% efficiency, respectively, while GFP plasmids were successfully delivered and expressed. These platforms open the way for active, reproducible delivery of a wide variety of species into cells without endocytosis.

KEYWORDS: Nanobiotechnology, biointerfaces, intracellular delivery, drug delivery, high-throughput bioassay
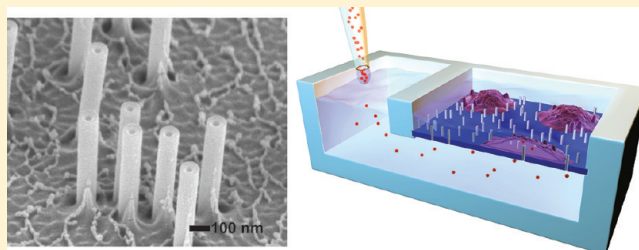
Methods for cytosolic delivery of biomolecules are essential for a broad range of modern biological and biomedical techniques, including siRNA knockouts, cell reprogramming, intracellular imaging, and pharmaceutical therapeutics.[1−5] Biological processes are often harnessed to transfer reagents across the cell membrane barrier, such as viral vectors for gene delivery[1,6] and endocytotic uptake of cargo, using carriers such as lipofectamine.[3−5,7] However, these methods are hampered by lysosomal degradation, cell-type specificity, low efficiency, expense, or toxicity concerns.[8,9] This has led to more physical approaches to directly breach the cell membrane. Techniques such as electroporation or micropipetting can be highly efficient, yet these suffer from their own drawbacks including low cell viability and low throughput, respectively.[10,11]

Recently, nanomaterial platforms have been used to improve intracellular delivery. While two-dimensional surface patterning and texturing have long been used to influence cell behavior,[12−14] high-aspect ratio nanowires have opened an entirely new avenue for cellular interaction due to their potential for direct membrane penetration.[15−18] By functionalizing nanowires with bioactive molecules, intracellular delivery has been demonstrated[19,20] while maintaining cell viability and behavior.[21] These exciting new methods are very promising, yet are restricted to molecules that can be linked or otherwise bound to the nanowires and offer little temporal or concentration control. Alternatively, functionalized scanning probes or pipettes can be used to inject selected cells,[22−24] but these serial processes are cumbersome for large numbers of cells.

Biological systems have developed blueprints for stable conduits through the cell wall. These include gap junction proteins that facilitate intercellular diffusion of chemical species between eukaryotic cells,[25,26] and ∼100 nm diameter hollow lipid nanotubes between bacteria, which transmit proteins and confer antibiotic resistance to neighboring bacteria.[27] These nanoscale intercellular junctions provide fluidic access and promote molecular exchange, yet are small enough to avoid cell toxicity.

Inspired by this design, we report a simple biomimetic "nanostraw" platform that establishes continuous fluidic access into the cell interior for the delivery of small molecules, proteins, and genetic material (Figure 1a). Cells cultured on nanostraws of sufficiently small diameter (∼100 nm) are spontaneously penetrated, creating externally controlled fluidic conduits into the cell that are stable over days. Time-resolved, sequential deliveries can be carried out without the need to continually rupture the cell membrane. Intracellular delivery of molecules ranging from ions to 5000 base pair DNA constructs is possible with subminute temporal resolution within a simple-to-use sample well platform. The stability, versatility, and nonperturbative nature of the nanostraws provide a uniquely powerful, yet subtle tool to access the inner clockwork of the cell.

Nanostraws were fabricated starting with track-etched polycarbonate membranes,[28] widely used for cell-culture and water purification,[29,30] as a template. These membranes are commercially available (AR Brown-US, Long Beach, CA) in a range of pore sizes (∼20 nm to 10 μm) and pore densities. In this study, devices were fabricated with membrane pore diameters ranging from 100 to 750 nm and pore densities of 10^6, 10^7, and 10^8 pores/cm^2 (Figure 1b). First, an alumina coating was deposited on all nanoporous membrane surfaces (top, bottom, and inside the pores) with atomic layer deposition (ALD),[31] yielding a uniform coating, typically chosen to be 10−30 nm thick (Figure 1c). The deposited alumina creates the nanostraw bodies within the nanopore interiors and defines the nanostraw
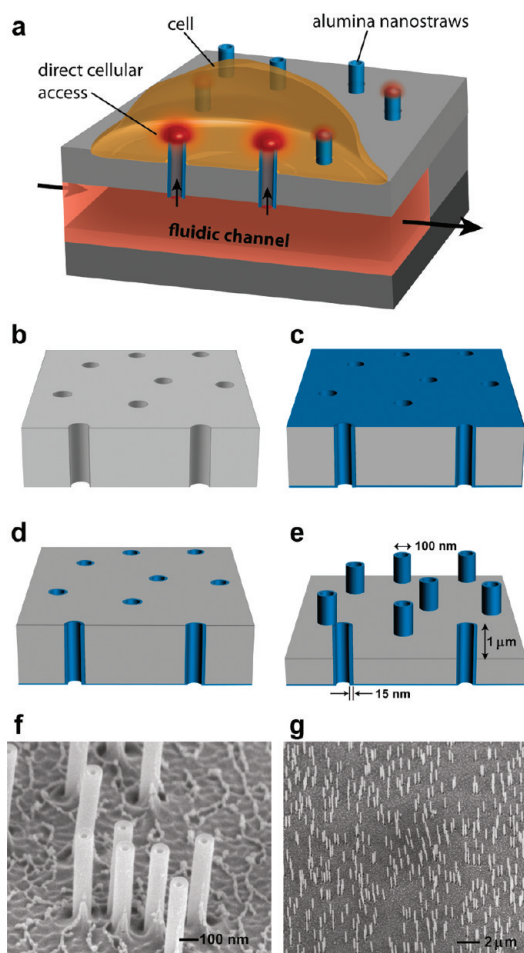
Figure 1. Nanostraw−cell interfacing strategy and fabrication. (a) Schematic of cell cultured on nanostraw membrane with microfluidic channel access. (b−e) Straw fabrication process flow begins with a nanoporous polycarbonate membrane (b), proceeds with conformal alumina atomic layer deposition (c), then an alumina specific directional reactive ion etch (d), and concludes with a polycarbonate specific directional reactive ion etch (e). (f,g) Scanning electron micrographs of nanostraw membranes.

wall thickness. Next, the alumina on the top surface was removed with a directional reactive ion etch (RIE) to expose the bare polymer layer underneath (Figure 1d). Finally, an oxygen RIE was used to expose the nanostraws by selectively etching the polymer until the desired nanostraw height was obtained, typically 1−2 μm (Figure 1e). The oxygen RIE is highly selective for polycarbonate membrane, ensuring that the alumina comprising the nanostraws is not degraded as the straws are created.

The nanostraw dimensions are independently controllable though adjustments to the track-etched membrane properties (straw diameter and density), ALD alumina thickness (straw wall thickness), and etch time (nanostraw height). These micro-fabrication processing steps can easily create large area, 100 mm Petri-dish size sheets of nanostraws. Scanning electron microscopy (SEM) confirmed that the process yields well-defined nanostraws on the top side of the membranes for all membranes tested (Figure 1f,g and Supporting Information Figure S1). The nanostraw height, wall thickness, and inner diameter were highly uniform with less than 5% variation as measured from scanning electron microscope images on sample

areas spaced over 1 cm apart. Nanostraws with aspect ratios as high as 10:1 were created with essentially quantitative yields. The dimensions of the smallest nanostraw diameters (100 nm) are comparable to those of nanowires previously used for direct delivery,[20] while the largest diameters (750 nm) resemble structures used for neural interfacing.[32] The oxygen etch leaves a slightly textured polycarbonate surface (Figure 1f), however this did not adversely affect cell culture.

The track-etched nanoporous membrane template is advantageous for several reasons. First, it is commonly available and commercially sold as a cell culture substrate. Second, the nanopores are available in a wide range of relatively mono-disperse diameters and pore densities, though the actual position of the straws relative to each other is stochastic. Controlling straw density is important, as cells appear to remain suspended on the top of high-density arrays of nanotubes (>10⁹) and are not penetrated.[33] Finally, the "self-aligned" fabrication process ensures that each nanostraw is fluidically connected to the bottom of the membrane without the need for top-down nanostraw-pore alignment. Further fabrication steps can also introduce different material layers within the nanostraws, or surface-modify the alumina as desired.

Reagent delivery through the nanostraws and into penetrated cells is regulated by controlling the solution composition underneath the polymer/nanostraw membrane. This could be as simple as suspending the membrane over a small dish with the desired solution (Figure 2a) or integrating the membrane on
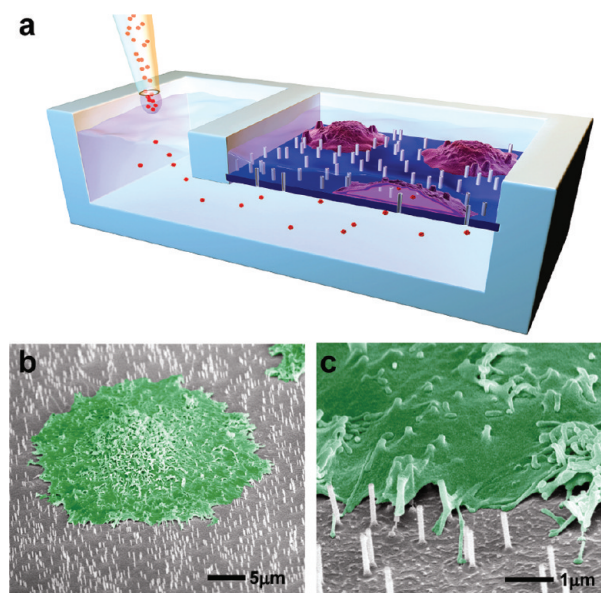
Figure 2. Device schematic overview. (a) A cross section of a typical device used to deliver biomolecules into cells via nanostraw-mediated delivery. (b,c) SEM images of critical point dried (CPD) cells cultured on nanostraw membranes (false colored green) with 100 nm diameter straws at a density of 10^8 straws/cm².

top of a microfluidic channel for rapid solution exchange or spatial concentration gradients (Figure 1a). In this study, the nanostraw membrane is placed on top of two different fluidic devices depending on the number of cells required. For spatially selective delivery, the membrane is suspended over a microfluidic channel 0.25−1 mm wide, ~100 μm deep, and ~1 cm long. For large cell cultures, the nanostraw membrane is supported over a single fluidic chamber approximately 1 cm × 1 cm × 0.1 cm in

size with an external access tube. A second PDMS layer with a cut-out area defining the cell culture region (sized slightly smaller than the nanostraw membrane) is then bonded on top. Solutions introduced into the fluidic channel beneath the membrane diffusively travel through the nanostraws, either into a cell or the cell culture area. A similar platform for extracellular chemical delivery without the nanostraws was recently reported and it was found that molecular delivery rates agreed with analytical diffusion models.[34] Simple one-dimensional diffusion calculations estimate that small molecules such as ions ($D \sim 100\ \mu m^2/s$) should diffuse through the 10 μm thick polymer membrane and straws in $\sim$50 s, while larger proteins ($D \sim 10\ \mu m^2/s$) may take up to 10 min.

After microfluidic integration, the device is flushed with bovine serum albumin (BSA) to minimize reagent adhesion to the walls, and cells are plated onto the nanostraws. Note that cells may simply be added on top of the nanostraw membrane, avoiding complications of injection or encapsulation in microfluidic chambers. Both HeLa and CHO cells cultured in 10% serum spread normally on the nanostraws compared with control samples without nanostraws, even proliferating and dividing at longer time scales (Figure 2b,c and Supporting Information Figures S2, S3). Cells grew equally well on nanostraw membranes supported on PDMS and suspended over fluid.

We demonstrate direct fluidic access to the cytosol through the nanostraws by the delivery of membrane-impermeable fluorescent dyes, ions, and green fluorescent protein (GFP) plasmid, which would normally be blocked by the cell membrane. These molecules, along with RNA, large proteins, and many other biomolecular tools used in cell studies, are generally unable to enter the cytosol without a transport agent.[35] Figure 3a shows cells dyed with Alexa-Fluor 488-hydrazide, a membrane-impermeant dye. Cells were allowed to adhere for one hour on a large-area cell culture device before the dye was introduced into the underlying fluidic chamber for a fixed period. Dye delivery was maintained over 4 and 24 h for nanostraw platforms with 10^8 and 10^7 straws/cm^2, respectively. The culture media was periodically replaced to suppress nonspecific dye uptake. At the end of the delivery period, cells were trypsinized, replated, and imaged, as in situ imaging was hampered by the background fluorescence of dye adsorbed to device walls. Cells cultured on large (250 and 750 nm) diameter straws were exposed to higher dye concentrations than cells cultured on 100 nm diameter nanostraws due to higher molecular flux through the nanostraws. However, cells cultured on these large straws did not show dye uptake, while cells on 100 nm straws showed significant fluorescence (Figure 3a). This fluorescence increase indicates that 100 nm diameter straws penetrate the cell membranes, while larger straws do not. This result agrees with previously reported work, where $\sim$100 nm diameter nanowires were used to successfully deliver biomolecules into cells.[20] Increasing the straw density from 10^7 to 10^8 straws per cm^2 decreased the time required for delivery, although more frequent media replacement was also necessary. Control experiments on polymer membranes without nanostraws were marked by very weak fluorescent staining, consistent with low-level endocytotic uptake (Figure 3b). Nanostraw-mediated delivery was also not limited to one cell type, as both HeLa and CHO cells were successfully dyed.

Since cell membranes are highly dynamic and can self-heal transient membrane pores,[36] whether the nanostraw-cytosol connection remains open after the initial penetration event is an important question. A stable fluidic interface is highly preferable for temporal control of chemical delivery and could
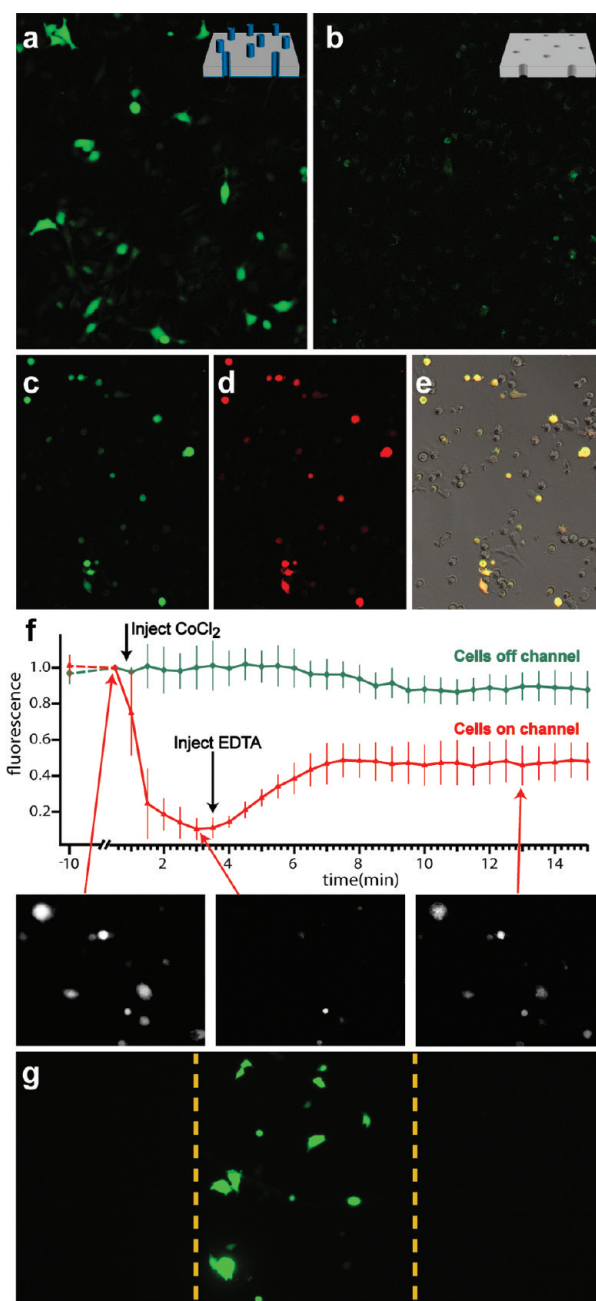
Figure 3. Epifluorescence images of molecular delivery into cells. Epifluorescence micrographs of replated cells after 24 h delivery of Alexa-Fluor 488-hydrazide membrane impermeant dye (a) with a nanostraw membrane and (b) with a nanostraw free membrane. After dye delivery through nanostraws, the cells demonstrate various levels of cell penetration and cytosolic fluorescence. An epifluorescence micrograph of (c) Alexa-Fluor 488-hydrazide dye delivered for 24 h, (d) Alexa-Fluor 568-hydrazide dye sequentially delivered 12 h after Alexa-Fluor 488-hydrazide dye, and (e) a composite image demonstrating colocalization of dyes. (f) A comparison between the fluorescence intensity in GFP expressing cells on and off the flow channel during delivery of a CoCl$_2$ quenching agent, and then an EDTA dequencher. Points are fluorescence intensity averages of eight successful cells normalized to the intensity at $t = 0$. Error bars indicate ± 1 SD. (g) Nanostraw-mediated GFP transfection of CHO cells cultured over a microfluidic channel (defined by dashed lines) 72 h after plasmid delivery.

even enable extraction and external detection of cytosolic proteins. We tested the stability of the nanostraw fluidic interface by delivering two different membrane-impermeable dyes at

prescribed time intervals (Figure 3c−e). In this experiment, if cells that accept the first dye (Alexa-Fluor 488-hydrazide, green) do not accept the second (Alexa-Fluor 568-hydrazide, red), then the interface sealed over the time period between deliveries and is therefore not stable. We tested this hypothesis by delivering the second dye either 2 or 12 h after the first dye, again for devices with straw densities of 10^8 and 10^7 straws/cm^2, respectively. As shown in Figure 3c−e, the dyes colocalized in >99% of cells, demonstrating that the fluidic interface remains open and stable over extended periods. Interestingly, the stained cells displayed several different fluorescence intensities, suggesting that the number of penetrating straws per cell may vary. The cell intensities generally followed an exponential or Poisson distribution, implying that cell membrane penetration is a stochastic process that we estimate to be roughly 1−10% efficient per nanostraw. However, as there are tens to hundreds of nanostraws underneath a typical 10 μm × 10 μm adherent cell at straw densities of 10^7−10^8, overall delivery success per cell can be over 70%.

A high degree of spatial and temporal control over chemical delivery is made possible by using microfluidic technology to control the solution composition beneath the nanostraws.[37] Time-resolved delivery is valuable as it allows for more flexibility in experimental design, greater control over the cellular environment, and finer resolution for investigating cellular response to a signal. Temporal control of nanostraw mediated delivery was investigated through fluorescence quenching and recovery observed in situ. Constitutively GFP-expressing CHO cells were plated in serum onto nanostraws to establish fluidic access and then exposed to pulses of CoCl$_2$ and ethylenediamine-tetra-acetic acid (EDTA) to quench and dequench GFP fluorescence. Co^{2+} quenches fluorescence[38] but must be delivered directly to the cytosol due to low trans-membrane permeability. Subsequent introduction of EDTA into the cells complexes free Co^{2+}[39] and results in partial fluorescence recovery. Fluorescence imaging before, during, and after quenching demonstrated that only cells positioned over the microfluidic channel were affected (Supporting Information Figure S4). This spatial selectivity confirms that extracellular CoCl$_2$ in the cell culture solution (present due to diffusion through nanostraws not penetrating cells) was insufficient for fluorescence quenching and that direct nanostraw delivery of Co^{2+} into cells was responsible. These cells were marked by significant reductions in fluorescence within one minute of Co^{2+} introduction in the microfluidic channel (Figure 3f). Subsequent delivery of EDTA allowed 75% of quenched cells to regain fluorescence over roughly four minutes. This fluorescent "blinking" demonstrates direct external manipulation of intracellular content using nanostraws on the time scale of tens of seconds.

We used the delivery of GFP plasmid as a functional assay and a demonstration that a relatively large molecular weight species (~5000 bp construct) can be delivered with nanostraws (Figure 3g). GFP plasmid delivery was performed similarly to small molecule delivery by introducing 0.37 μg/μL plasmid in PBS into the microfluidic channel and allowing 24 h for cell uptake and expression. At the end of this period cells were imaged in a fluorescent microscope without replating. Since GFP-plasmid is not fluorescent, cells could be imaged directly on the nanostraw substrates. Figure 3g shows that ~5−10% of cells located over the microfluidic channel are successfully transfected, while 0% of cells off the channel are transfected.

The spatial confinement confirms that nanostraws are necessary as membrane-penetrating conduits for intracellular delivery.

The efficiency of nanostraw-mediated delivery varies across different experiments and molecules. Low molecular weight species, such as ions, are expected to be highly effective as they are small, have high diffusivity, and do not greatly adsorb to channel or straw sidewalls. Delivery of Co^{2+} ions in in situ tests of GFP quenching was found to be 70.3% efficient (n = 108), indicating a majority of cells are penetrated by one or more nanostraws. For long-term molecular deliveries, lower yields of 20−40% were observed for ex situ replated cells. In situ observation of GFP transfection resulted in yields of 5−10%. The efficiency of GFP expression relative to Co^{2+} ion delivery is attributed to GFP plasmids having high surface affinity, lower diffusivity, and the additional biochemical translation and expression steps necessary. Delivery efficiency was also dependent on nanostraw density with maximum delivery observed at straw concentrations between 10^7−10^8/cm^2. The ideal straw density is a compromise between two competing effects, as lower straw concentrations result in lower total molecular flux through the membrane, while very high nanostraw densities result in less frequent cell penetration, as cells rest on top of the dense nanostraw forest with a bed-of-nails effect.[33]

We compared nanostraw-mediated dye delivery to dye uptake though other possible pathways to verify the role of nanostraws as membrane-spanning conduits. One concern is that nanostraws not penetrating into cells deliver molecules into the upper cell culture solution. Cells are well-known to uptake molecules from solution through endocytosis,[8,40−42] which can be difficult to distinguish from direct delivery (Figure 4a). However, endocytotic dye uptake of membrane impermeable dyes is characterized by spatially confined points of fluorescence within the cell where dye is enclosed in discrete endocytotic vesicles, as opposed to uniform cytosolic distribution expected from direct delivery.[43] To confirm that nanostraw-mediated dye delivery was not endocytotic, cells were imaged using confocal microscopy to determine the dye distribution (Figure 4b−e). Alexa-Fluor 488-hydrazide dye (green) was delivered through the nanostraws, resulting in homogeneous cell-body fluorescence in selected cells (Figure 4b). Simultaneous addition of Alexa-Fluor 568-hydrazide (red) into the upper culture well resulted in punctate vesicular fluorescence of red dye in all cells (Figure 4b). These contrasting patterns of continuous and punctate fluorescence, as well as the difference in cell-to-cell staining (stochastic for nanostraws, consistent for endocytosis), highlight that extracellular dye uptake and nanostraw dye delivery operate on different principles. These delivery patterns were also preserved when nanostraw-mediated dye delivery and endocytotic uptake of dye were observed independently (Figure 4c,d). Confocal image slices showed uniform dye distribution throughout the entire cell bodies in the z-direction with nanostraw-mediated delivery, again in contrast to punctate fluorescence observed in cells cultured with dye-supplemented media. When dye was delivered to cells through track-etched membranes without straws, the observed fluorescence pattern in confocal microscopy was also punctate (Supporting Information Figure S5), highlighting once more that nanostraws are needed to form direct conduits to the cellular interior.

The possibility that nanostraws puncture the cell membrane and allow extracellular molecules to diffuse into the cytosol must also be considered, as nonspecific leakage could provide an alternative pathway into the cell.[44] Leakage could occur at the nanostraw−cell interface, where the membrane must form a
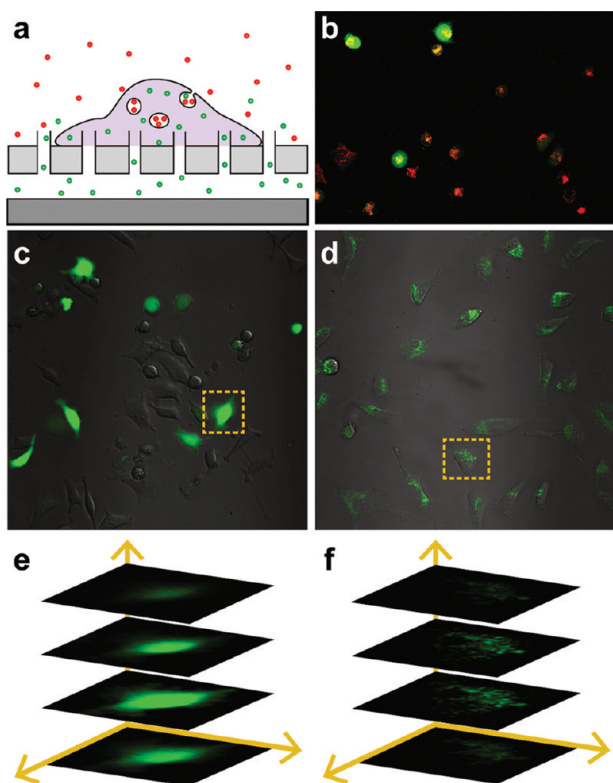
Figure 4. Nanostraw-mediated and nonspecific endocytotic dye delivery result in different localization patterns within cells. Endocytotic uptake results in localized points of fluorescence as dye is confined in vesicles, which is in contrast to diffuse nanostraw-mediated delivery (a). Confocal microscopy shows that all cells exhibit vesicular fluorescence while a subset of cells exhibit cytosolic fluorescence (b). When uptake methods are observed independently, cells still exhibit cytosolic fluorescence (c) after nanostraw-mediated delivery, and vesicular fluorescence (d) when cultured in dye-supplemented media. Z-slices of a characteristic cell show that this difference in dye distribution is observed throughout the entire cell body for nanostraw-mediated delivery (e, dashed box in c), and endocytosis from dye-supplemented media (f, dashed box in d).

seal around the piercing nanostraw. This pathway is less likely due to the very significant differences in delivery efficiency between cells located over the fluidic channel and those over PDMS, even though they both share the same culture solution. This effect should have been especially dramatic for molecular ions due to their small size and high diffusion constants, however, GFP quenching by Co^{2+} ions was strictly confined to cells directly over the channel, casting further doubt on this mechanism.

Cells cultured on nanostraw platforms remained viable and proliferated based on optical microscopy and live/dead staining (Supporting Information Figure S2). More subtle changes in cellular behavior were probed by mRNA expression analysis.[45] Gene chip analyses were compared between cells grown on nanostraw membranes and nanostraw-free membranes at time points of 2 h, 3 days, and 5 days. Several cell functions were considered prime targets for genetic up-regulation among cells grown on nanostraws, including indicators of cell stress, endocytosis, and ion channel regulation. Cell stress is a common result of unusual culture conditions, including surface modification;[46] up-regulated endocytosis is a proposed mechanism for impalefection via high-aspect nanowires;[8] and increased ion channel activity may be necessary to maintain the cell membrane potential if nanowire

penetration results in ionic leakage.[47] However, examination of genes associated with these cell functions[48] reveals no expression changes greater than 1.21-fold (Figure 5a−c), considered
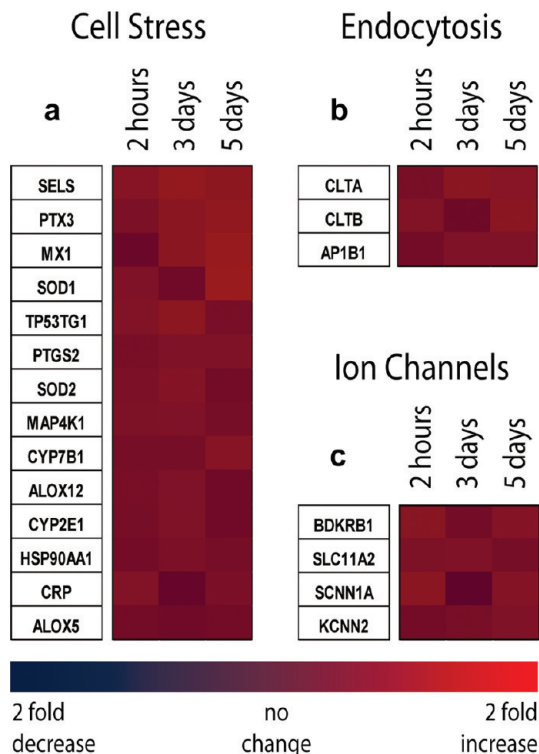
Figure 5. Cells cultured on membranes with and without nanostraws shows minimal change in gene expression. Heat maps for genes associated with (a) cell stress, (b) endocytosis, and (c) ion channels, demonstrate negligible changes in expression.

statistically equivalent. This observation corroborates prior observations that high-aspect ratio nanostructure-cell interactions result in minimal cell perturbation.[20] Additionally, a Pearson correlation analysis of all 28 869 genes examined showed that in every instance, the differences between how long the cells were in culture was the most influential factor in mRNA expression variation, rather than the presence or absence of nanostraws (Supporting Information Figure S6). These data suggest that nanostraws, which are present at relatively low densities in comparison to nanostructures used in other recent studies,[21,45] exert relatively minor pressure on gene expression levels.[20]

The nanostraw platform leverages nanofabrication for in vitro biological studies by delivering membrane-impermeable species directly into the cell cytosol with minimal perturbation. Unlike traditional delivery methods, nanostraw platforms combine long-term access, temporal control, low cellular disruption, and ready integration into microfluidic systems into a single device. These are important steps toward complete regulation and monitoring of internal cell dynamics. A wide range of current cell culture platforms can be powerfully augmented using nanostraw membranes, allowing biomolecule delivery in a massively parallel fashion over large areas. By nondestructively bypassing the cell's membrane barrier, nanostraw platforms may be able to alter the intracellular environment with the same degree of control that we currently exert over the extracellular solution, unlocking the full potential of engineered inorganic-cell communication.

ASSOCIATED CONTENT

ⓢ Supporting Information

Additional fabrication and experimental details. SEM images of additional nanostraws. Fluorescent images from live dead experiments, control experiments, and video and images of cell migration and division on nanostraws. Gene expression correlation chart for entire gene chip. This material is available free of charge via the Internet at http://pubs.acs.org.

AUTHOR INFORMATION

Corresponding Author

*E-mail: nmelosh@stanford.edu. Phone: 650-724-3679. Fax: 650-736-1984. Address: Geballe Laboratory for Advanced Materials, McCullough Building, Room 223, 476 Lomita Mall, Stanford University, Stanford, CA 94305-4045.

Author Contributions

‡These authors contributed equally.

ACKNOWLEDGMENTS

REFERENCES

(1) Tiscornia, G.; Singer, O.; Ikawa, M.; Verma, I. M. *Proc. Natl. Acad. Sci. U.S.A.* **2003**, *4*, 1844−1848.

(2) Plath, K.; Lowry, W. E. *Nat. Rev. Genet.* **2011**, *4*, 253−265.

(3) Michalet, X.; Pinaud, F. F.; Bentolila, L. A.; Tsay, J. M.; Doose, S.; Li, J. J.; Sundaresan, G.; Wu, A. M.; Gambhir, S. S.; Weiss, S. *Science* **2005**, *5709*, 538−544.

(4) Carter, P. J. *Nat. Rev. Immunol.* **2006**, *5*, 343−357.

(5) Heath, J. R.; Davis, M. E. *Annu. Rev. Med.* **2008**, 251−265.

(6) Hanna, J.; Saha, K.; Pando, B.; van Zon, J.; Lengner, C. J.; Creyghton, M. P.; van Oudenaarden, A.; Jaenisch, R. *Nature* **2009**, *7273*, 595−601.

(7) Choi, M.; Stanton-Maxey, K. J.; Stanley, J. K.; Levin, C. S.; Bardhan, R.; Akin, D.; Badve, S.; Sturgis, J.; Robinson, J. P.; Bashir, R.; Halas, N. J.; Clare, S. E. *Nano Lett.* **2007**, *12*, 3759−3765.

(8) Adler, A. F.; Leong, K. W. *Nano Today* **2010**, *6*, 553−569.

(9) Luo, D.; Saltzman, W. M. *Nat. Biotechnol.* **2000**, *1*, 33−37.

(10) Chu, G.; Hayakawa, H.; Berg, P. *Nucleic Acids Res.* **1987**, *3*, 1311−1326.

(11) Susin, S.; Lorenzo, H.; Zamzami, N.; Marzo, I.; Snow, B.; Brothers, G.; Mangion, J.; Jacotot, E.; Costantini, P.; Loeffler, M.; Larochette, N.; Goodlett, D.; Aebersold, R.; Siderovski, D.; Penninger, J.; Kroemer, G. *Nature* **1999**, *6718*, 441−446.

(12) Kubota, Y.; Kleinman, H. K.; Martin, G. R.; Lawley, T. J. *J. Cell Biol.* **1988**, *4*, 1589−1598.

(13) Ruoslahti, E.; Pierschbacher, M. D. *Science* **1987**, *4826*, 491−497.

(14) James, C. D.; Davis, R. C.; Kam, L.; Craighead, H. G.; Isaacson, M.; Turner, J. N.; Shain, W. *Langmuir* **1998**, *4*, 741−744.

(15) Kim, W.; Ng, J. K.; Kunitake, M. E.; Conklin, B. R.; Yang, P. *J. Am. Chem. Soc.* **2007**, *23*, 7228−7229.

(16) Yang, P.; Yan, R.; Fardy, M. *Nano Lett.* **2010**, *5*, 1529−1536.

(17) Tian, B.; Cohen-Karni, T.; Qing, Q.; Duan, X.; Xie, P.; Lieber, C. M. *Science* **2010**, *5993*, 830−834.

(18) Xie, C.; Hanson, L.; Cui, Y.; Cui, B. *Proc. Natl. Acad. Sci. U.S.A.* **2011**, *10*, 3894−3899.

(19) McKnight, T. E.; Melechko, A. V.; Hensley, D. K; Mann, D. G. J.; Griffin, G. D.; Simpson, M. L. *Nano Lett.* **2004**, *7*, 1213−1219.

(20) Shalek, A. K.; Robinson, J. T.; Karp, E. S.; Lee, J. S.; Ahn, D.; Yoon, M.; Sutton, A.; Jorgolli, M.; Gertner, R. S.; Gujral, T. S.; MacBeath, G.; Yang, E. G.; Park, H. *Proc. Natl. Acad. Sci. U.S.A.* **2010**, *5*, 1870−1875.

(21) Qi, S.; Yi, C.; Ji, S.; Fong, C.; Yang, M. *ACS Appl. Mater. Interfaces* **2009**, *1*, 30−34.

(22) Chen, X.; Kis, A.; Zettl, A.; Bertozzi, C. R. *Proc. Natl. Acad. Sci. U.S.A.* **2007**, *20*, 8218−8222.

(23) Loh, O.; Lam, R.; Chen, M.; Moldovan, N.; Huang, H.; Ho, D.; Espinosa, H. D. *Small* **2009**, *14*, 1667−1674.

(24) Singhal, R.; Orynbayeva, Z.; Sundaram, R. V. K.; Niu, J. J.; Bhattacharyya, S.; Vitol, E. A.; Schrlau, M. G.; Papazoglou, E. S.; Friedman, G.; Gogotsi, Y. *Nat. Nanotechnol.* **2011**, *1*, 57−64.

(25) Kumar, N. M.; Gilula, N. B. *Cell* **1996**, *3*, 381−388.

(26) Alberts, B.; Johnson, A.; Lewis, J.; Raff, M.; Roberts, K.; Walter, P. *Molecular Biology of the Cell*, 4th ed.; Garland Science: New York, 2002.

(27) Dubey, G. P.; Ben-Yehuda, S. *Cell* **2011**, *4*, 590−600.

(28) Martin, C. R. *Science* **1994**, *5193*, 1961−1966.

(29) Keenan, T. M.; Folch, A. *Lab Chip* **2008**, *1*, 34−57.

(30) Bernards, D. A.; Desai, T. A. *Soft Matter* **2010**, *8*, 1621−1631.

(31) Feng, H.; Elam, J. W.; Libera, J. A.; Pellin, M. J.; Stair, P. C. *Chem. Eng. Sci.* **2009**, *3*, 560−567.

(32) Zeck, G.; Fromherz, P. *Proc. Natl. Acad. Sci. U. S. A.* **2001**, *18*, 10457−10462.

(33) Popat, K. C.; Leoni, L.; Grimes, C. A.; Desai, T. A. *Biomaterials* **2007**, *21*, 3188−3197.

(34) VanDersarl, J. J.; Xu, A. M.; Melosh, N. A. *Lab Chip* **2011**, *11*, 3057−3063.

(35) Langer, R. *Nature* **1998**, *6679*, 5−10.

(36) Bier, M.; Hammer, S.; Canaday, D.; Lee, R. *Bioelectromagnetics* **1999**, *3*, 194−201.

(37) El-Ali, J.; Sorger, P. K.; Jensen, K. F. *Nature* **2006**, *7101*, 403−411.

(38) Petronilli, V.; Miotto, G.; Canton, M.; Brini, M.; Colonna, R.; Bernardi, P.; Di Lisa, F. *Biophys. J.* **1999**, *2*, 725−734.

(39) Brady, D.; Duncan, J. *Appl. Microbiol. Biotechnol.* **1994**, *1*, 149−154.

(40) Verma, A.; Uzun, O.; Hu, Y.; Hu, Y.; Han, H.; Watson, N.; Chen, S.; Irvine, D. J.; Stellacci, F. *Nat. Mater.* **2008**, *7*, 588−595.

(41) Peckys, D. B.; de Jonge, N. *Nano Lett.* **2011**, *4*, 1733−1738.

(42) Bhattacharyya, S.; Bhattacharya, R.; Curley, S.; McNiven, M. A.; Mukherjee, P. *Proc. Natl. Acad. Sci. U.S.A.* **2010**, *33*, 14541−14546.

(43) Vasir, J. K.; Labhasetwar, V. *Adv. Drug Delivery Rev.* **2007**, *8*, 718−728.

(44) Malboubi, M.; Ostadi, H.; Wang, S.; Gu, Y.; Jiang, K. *Eng. Lett.* **2009**, *4*.

(45) Peng, L.; Barczak, A. J.; Barbeau, R. A.; Xiao, Y.; LaTempa, T. J.; Grimes, C. A.; Desai, T. A. *Nano Lett.* **2010**, *1*, 143−148.

(46) Gasiorowski, J. Z.; Liliensiek, S. J.; Russell, P.; Stephan, D. A.; Nealey, P. F.; Murphy, C. J. *Biomaterials* **2010**, *34*, 8882−8888.

(47) Black, J. A.; Cummins, T. R.; Plumpton, C.; Chen, Y. H.; Hormuzdiar, W.; Clare, J. J.; Waxman, S. G. *J. Neurophysiol.* **1999**, *5*, 2776−2785.

(48) Safran, M.; Dalah, I.; Alexander, J.; Rosen, N.; Iny Stein, T.; Shmoish, M.; Nativ, N.; Bahir, I.; Doniger, T.; Krug, H.; Sirota-Madi, A.; Olender, T.; Golan, Y.; Stelzer, G.; Harel, A.; Lancet, D. *Database* **2010**, DOI: 10.1093/database/baq020.